Macrophage-Targeting Poly(lactide-*co*-glycolic acid) Nanoparticles Decorated with Multifunctional Brush Polymers

Stephanie Christau[1,2], Aida López Ruiz[3], Nahal Habibi[1,2], Judith Witte[1,2], Mark S. Bannon[3], Kathleen McEnnis*[1,2,3], and Joerg Lahann*[1,2]

Dr. S. Christau, Dr. N. Habibi, Dr. J. Witte, Dr. K. McEnnis, Prof. J. Lahann

Department of Chemical Engineering, University of Michigan, 2800 Plymouth Rd, Ann Arbor, MI 48109, United States
E-mail: mcennis@njit.edu, lahann@umich.edu

Dr. S. Christau, Dr. N. Habibi, Dr. J. Witte, Dr. K. McEnnis, Prof. J. Lahann

Biointerfaces Institute, University of Michigan, 2800 Plymouth Rd, Ann Arbor, MI 48109, United States

E-mail: mcennis@njit.edu, lahann@umich.edu

A. López Ruiz, M. S. Bannon, Dr. K. McEnnis

Department of Chemical and Materials Engineering, New Jersey Institute of Technology, 161 Warren St., Newark, NJ, 07103, United States

E-mail: mcennis@njit.edu

Dr. J. Witte

Str. des 17. Juni 124, Technische Universitaet Berlin, 10623 Berlin, Germany

This study examines the potential of poly(lactic-co-glycolic acid) (PLGA) nanoparticles functionalized with poly(zwitterion)-mannose brushes to target macrophages. Uptake studies with RAW 264.7 macrophages indicated that multiple mannose binding sites in the grafted brushes facilitated interaction with the mannose receptor of the macrophages, resulting in approximately 4 times higher cellular uptake than nanoparticles with mannose monolayer coatings. To test the feasibility of the nanoparticles as long-circulating drug delivery vehicles, their multicomponent aggregation in blood plasma was analyzed using nanoparticle tracking analysis and compared to PEGylated particles, which are known to reduce aggregation. There was no significant difference in the aggregation behavior of the poly(zwitterion)-mannose grafted particles and the PEGylated control particles (~760 particles in aggregates per 10^5 particles). In addition, we compared the particle size in blood plasma, which includes the protein corona, after 0, 8, and 15 h. Whereas there was no significant difference at longer time scales, the overall particle size of the poly(zwitterion)-mannose brush-grafted nanoparticles was approximately 130 nm smaller than that of the PEGylated nanoparticles at shorter time scales, suggesting a smaller protein corona. All these results suggest that PLGA nanoparticles functionalized with poly(zwitterion)-mannose brush grafts may be excellent candidates for targeted drug delivery to macrophages.

1. Introduction

Nanomedicine is an emerging field, which employs nanomaterials to either prevent or treat disease; these materials include nanosensors for diagnostics, nanorobots, or drug-encapsulating nanocarriers.[1] In nanoparticle-based drug delivery, nanoscale materials are employed to deliver certain therapeutic agents to specific targeting sites. A major benefit of this approach lies in the ability to control the parameters of the nanocarrier, such as size, shape, density, or surface coating, which allows for a

controlled and sustained delivery of therapeutics.[2] Several types of nanocarriers to encapsulate drugs of interest have been developed for efficient drug delivery to the targeting site, including lipid nanoparticles,[3] inorganic nanoparticles,[4] protein-based nanoparticles,[5] and polymeric nanoparticles.[6] The appropriate carrier type is selected based on the desired drug release profile and also depends on the interactions between the drug and the carrier particle; drugs might be encapsulated by means of covalent bonding, hydrogen bonding interactions, electrostatic interactions, or van der Waals interactions.[1] Polyester-based nanoparticles (NPs), such as poly(lactic-co-glycolic acid) (PLGA) NPs, combine chemical versatility with degradability, and they are thus often studied as potential drug delivery vehicles[7, 8]. PLGA is an FDA-approved, biocompatible polymer, and PLGA NPs have been extensively studied for biomedical applications due to their tunable biodegradability, which allows for controlled and sustained release of encapsulated therapeutics[8-11]. In addition, the NP surface can be decorated with functional groups, such as targeting ligands, which allows for efficient delivery of therapeutics to a specific target. However, despite the advantageous properties of PLGA NPs, the therapeutic efficiency of nanoparticle-based drug delivery depends greatly on their stability in the bloodstream. Once injected, blood proteins adsorb onto the nanoparticle surface to form a protein corona that promotes opsonization and results in nanoparticle aggregation; this leads to rapid clearance of the nanoparticles from circulation via phagocytosis by the mononuclear phagocyte system (MPS).[12] The clearance mechanism involves receptor-mediated endocytosis of the opsonized nanoparticles by the cells of the liver and spleen. Thus, blood protein adsorption plays a crucial role in nanoparticle clearance by the liver. Protein adsorption leads to nanoparticle aggregation, which, due to the larger size of the particle clusters compared to the individual nanoparticles, facilitates their removal from the bloodstream. To prevent opsonization, aggregation and the resulting rapid clearance by the liver, the adsorption of blood proteins to the nanoparticle surface should therefore be avoided; one way to reduce protein adsorption and improve the blood circulation time is to decorate the nanoparticle surface with "stealth" groups such as poly(ethylene glycol) (PEG).[12-14]

Recently, macrophages have emerged as an attractive target in nanomedicine. Macrophages are phagocytic cells of the innate immune system; present in all tissues and organs, they are involved in maintaining tissue homeostasis and regulating inflammatory responses. There is a spectrum of macrophage phenotypes; traditionally, macrophages have been classified according to their activation state as M1- or M2-type macrophages.[15] M1-type macrophages, also referred to as classically activated macrophages, show efficient antigen presentation and release proinflammatory cytokines; on the other hand, M2 phenotypes, or alternatively activated macrophages, release anti-inflammatory

cytokines and are involved in tissue remodeling and wound healing, tumor growth, and angiogenesis.[16] Unlike M1-type macrophages, M2 phenotypes express mannose receptors (CD206), a 175 kDa integral membrane protein, which recognizes mannose, fucose and N-acetylglucosamine and has been utilized by researchers to target M2-type macrophages.[17] Targeting macrophages to intracellularly deliver drugs has gained recent clinical interest, as macrophages are used as host cells by pathogens causing intracellular infections, such as tuberculosis or salmonellosis.[18, 19] Previous studies have designed drug carrier particles for delivering antibacterial agents to macrophages.[18, 20] However, inefficient targeting and insufficient intracellular delivery of antibiotics remains an issue.[19] In addition, M2-type macrophages are associated with tumor growth and the development of fibrosis.[17] Efforts have been made to re-educate these macrophages,[21-23] a strategy that has emerged as a new and promising approach to tackle these diseases. To efficiently target these macrophages, mannosylation of the drug carrier (the conjugation of mannose moieties) is a commonly applied strategy; mannosylated NPs are recognized by the macrophage mannose receptor and internalized through pattern recognition receptor-mediated endocytosis.[24] There is evidence that a multivalent display of mannose moieties increases receptor recognition;[17, 25] for example, targeted delivery of antibiotics to macrophages was achieved using a nanogel with surface-conjugated PEG-mannose arms presenting multiple binding sites for the macrophage mannose receptor.[26] Further progress in the field has been hampered by the lack of well-defined nanoparticle models that efficiently engage with macrophages.

In addition to their targeting capability, the drug carriers need to be stable in physiological environment and exhibit an extended circulation time in the bloodstream. As mentioned earlier, the fate of nanoparticles in the bloodstream greatly depends on their interactions with blood proteins, which often results in aggregation; aggregation effectively causes an increase in size, resulting in removal of the nanoparticles from the bloodstream.[27-29] To avoid rapid clearance of the nanoparticles by the liver macrophages, PEGylation has been widely employed to prolong the circulation life of the nanoparticles and decrease their accumulation in the liver.[30-32] Other coatings have been investigated as well, and especially zwitterionic polymers have been shown to improve the NP circulation time.[33-37] In this work, we address the above-described challenges by developing multifunctional nanoparticles that (i) selectively target M2 macrophage phenotypes, while (ii) retaining stability in blood plasma. Importantly, we identify the molecular architecture of the zwitterionic surface coatings as key determinant of biological function and derive simple structure-function relationships.

We first compared the uptake of NPs functionalized with poly(carboxybetaine)-mannose by RAW 264.7 macrophages with the uptake of NPs coated with a simple mannose monolayer. The uptake of the brush-modified NPs was significantly higher than that of the monolayer-coated NPs, indicating that the presence of multiple mannose binding sites increased the recognition by the macrophages, which may improve the targeting efficacy. Next, we examined the NPs in terms of their aggregation behavior in blood plasma. An accurate quantification of NP aggregation in complex media, such as blood, is very difficult to achieve with commonly used methods like dynamic light scattering (DLS) since the components of blood also scatter light.[46, 47] Alternatively, nanoparticle tracking analysis (NTA), which tracks the motion of particles individually, can be employed.[48] This method has recently been successfully employed to quantify the aggregation behavior of PEGylated polystyrene nanoparticles in blood plasma.[49] Unlike DLS, NTA does not require a sample with monodisperse particles[46, 50] and thus allows for analysis of nanoparticle aggregation in blood. Aggregation in blood can occur between individual nanoparticles (homogeneous aggregation) and between the nanoparticles and blood proteins (multicomponent aggregation). The advantage of NTA analysis is that it can distinguish between homogeneous and multicomponent aggregation, which is important to make a statement regarding the performance of the drug carrier particle. In this work, we employed NTA to examine the aggregation behavior of the two mannosylated NP groups (mannose monolayer vs. poly(mannose) brush coatings) in blood plasma. In addition to the two mannosylated NP groups, we included PEGylated NPs, which are considered the "gold standard" for avoiding NP aggregation and prolonging the blood circulation time of the injected particles.[10, 51, 52]

2. Results and Discussion

2.1. Nanoparticle fabrication and characterization

2.1.1. Fabrication and characterization of PLGA NPs

The PLGA nanoparticles used in this study were fabricated by electrohydrodynamic jetting and subsequently surface-modified. We have used electrohydrodynamic jetting extensively in the past to prepare polymeric nanoparticles.[39-42] The NPs used in this study were prepared from a mixture of carboxy-terminated PLGA (for postmodification with PEG and mannose monolayers) and bromoisobutyrate-terminated poly(lactic acid) (PLA(BiBB)) (for postmodification with poly(carboxybetaine) brushes). Using this approach allowed us to prepare the different particle types

from the same particle batch, which is crucial because different batches may exhibit slightly different size, or zeta potential, which will ultimately also affect the aggregation behavior. To functionalize the PLGA NP surface with PEG or mannose monolayers, amine-PEG$_{1k}$ or amine-mannose, respectively, were reacted with the carboxy group of the PLGA/PLA(BiBB) via sulfo-NHS/EDC chemistry (**Figure 1**). To obtain the brush coating, we employed surface-initiated atom transfer radical polymerization (SI-ATRP) to grow poly(carboxybetaine) methacrylate (PCBMA) brushes, which were further reacted with amine-mannose, resulting in PCBMA-mannose brushes (Figure 1). The reason for this approach was twofold: We speculated that the presence of the zwitterionic polymers may not only allow for postmodification, but it may also be beneficial for preventing NP aggregation in the bloodstream, as poly(carboxybetaine) coatings have been proven effective in prolonging the blood circulation time of drug delivery vehicles.[34, 35, 43-45]
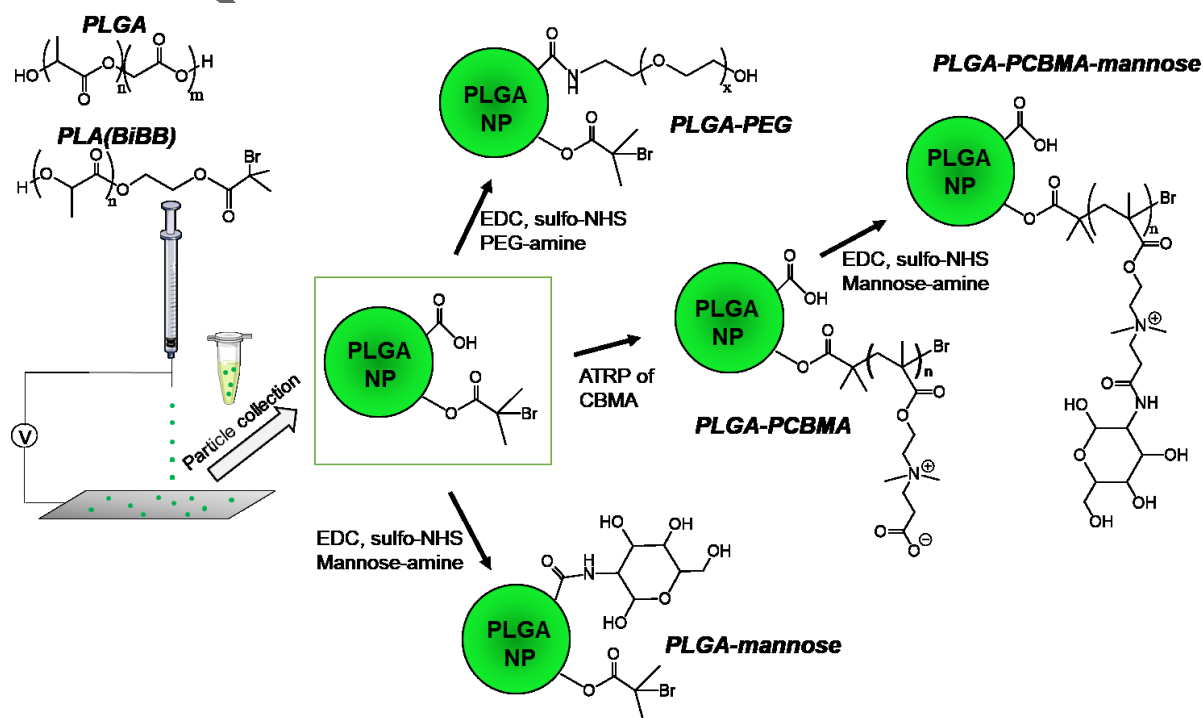

Figure 1. Surface modification of electrojetted PLGA nanoparticles: PEG and mannose monolayers were obtained via reaction with EDC/sulfo-NHS and amine-PEG$_{1k}$ or amine-mannose, respectively. PCBMA brushes were grown by SI-ATRP. PCBMA

brushes were post-modified with amine-mannose via EDC/sulfo-NHS chemistry to obtain PCBMA mannose brush coatings.

Fabrication of nanoparticles with tunable PLGA/PLA(BiBB) ratios allows for synthesis of brushes with varying grafting densities; specifically, increasing the PLA(BiBB) amount should result in a higher brush grafting density on the nanoparticle surface (however, an evaluation of different grafting densities was not the scope of the current study). We hypothesized that the PLGA/PLA(BiBB) ratios might not only affect the resulting brush grafting density, but also influence the electrohydrodynamic jetting process due to the different solubilities of PLGA and PLA(BiBB) in the solvent mixture. Indeed, we found that increasing the amount of PLA(BiBB) in the formulation reduced the particle yield, as evident from the SEM images of the PLGA nanoparticles doped with 5% PLA(BiBB) (**Figure 2**). Decreasing the PLA(BiBB) amount from 5% to 2.5%, or 1% resulted in higher yields compared with the formulation with 5% PLA(BiBB).

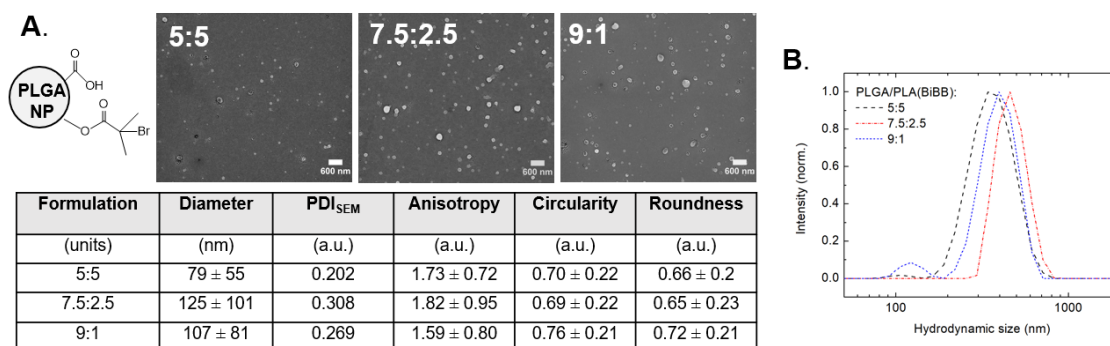| Formulation	Diameter	PDI$_{SEM}$	Anisotropy	Circularity	Roundness
(units)	(nm)	(a.u.)	(a.u.)	(a.u.)	(a.u.)
5:5	79 ± 55	0.202	1.73 ± 0.72	0.70 ± 0.22	0.66 ± 0.2
7.5:2.5	125 ± 101	0.308	1.82 ± 0.95	0.69 ± 0.22	0.65 ± 0.23
9:1	107 ± 81	0.269	1.59 ± 0.80	0.76 ± 0.21	0.72 ± 0.21

Figure 2. (A.) SEM images of nanoparticles consisting of PLGA/PLA(BiBB) ratios (wt%) of 7.5:2.5, 5:5 and 9:1. The table shows the nanoparticle diameter, PDI$_{SEM}$, anisotropy, circularity, and roundness obtained from SEM image analysis (ImageJ). (B.) Hydrated nanoparticle size measured by DLS after nanoparticle collection in PBS and centrifugation at 12,700 RCF for 1 min.

SEM images provide a first examination of the nanoparticles with respect to their size and shape (**Figure 2**). At a first glance, the nanoparticles appear spherical regardless of the formulation used, and they appear to be of similar size with a certain degree of polydispersity. A more detailed analysis of the SEM images of the as-electrojetted nanoparticles was conducted with FIJI (a distribution of ImageJ v1.53c). For each nanoparticle formulation, multiple SEM images were analyzed (for a total

7

of 500 particles) to obtain their size distribution and an SEM-based PDI value (PDI$_{SEM}$), which was generated as described previously.[53] In addition to the size distribution of the nanoparticles, we determined secondary geometric factors including nanoparticle circularity, roundness and anisotropy. The average diameters of the PLGA NPs containing 5, 2.5 and 1 w/w% PLA(BiBB) were ~79 nm, ~125 nm and ~107 nm, and the corresponding PDI$_{SEM}$ values were 0.202, 0.308 and 0.269, respectively. Statistical analysis found that the diameters were significantly different for all formulations (see supporting information). The analysis of the abovementioned secondary geometric factors determined anisotropy values ranging from 1.59 to 1.82, circularity values ranging from 0.69 to 0.76, and roundness values ranging from 0.65 to 0.72. There were statistical differences in the anisotropy, circularity and roundness values between the formulations with 1 w/w% PLA(BiBB) and 2.5 or 5 w/w% PLA(BiBB). There was no statistical difference between the formulations with 2.5 w/w% PLA(BiBB) and 5 w/w% PLA(BiBB) (see supporting information).

To evaluate the particle characteristics in their hydrated state, the nanoparticles were collected in PBS containing 0.1 v/v% Tween20 with a razor blade. As indicated by the SEM image analysis, there is a certain degree of polydispersity (0.202 – 0.308) of the as-electrojetted nanoparticles. In polydisperse samples, larger particles can be recovered using shorter centrifugation times, while the smaller particles require longer centrifugation times. In this study, we were only interested in NPs with ~400-600 nm hydrated diameter due to the detection limit of fluorescent samples in NTA. We found that centrifugation of the collected nanoparticles at 12,700 RCF for 1 min yielded the desired particle size; the smaller NPs remaining in the supernatant were discarded. The hydrated size of the NPs after this centrifugation step was measured by DLS (Figure 2), and values of 383 nm, 472 nm, and 415 nm diameter were obtained for the PLGA NPs doped with 5%, 2.5% and 1% PLA(BiBB).

2.1.2. Characterization of surface-modified PLGA NPs

Since we did not notice any significant differences in the electrohydrodynamic jetting process of PLGA nanoparticles doped with 1% or 2.5% PLA(BiBB), we chose the formulation containing 2.5% PLA(BiBB) to prepare the PLGA NPs for postmodification with monolayers and brushes. To fluorescently label the nanoparticles for the NTA experiments, a polymeric green dye (ADS133YE) was added to the solution containing PLGA, PLA(BiBB), and CTAB before electrohydrodynamic jetting. The incorporation of the dye did not affect the hydrated size of the resulting PLGA NPs, which was determined after centrifugation at 12,700 RCF for 1 min by DLS as 497 nm. Next, this batch of the PLGA NPs was divided into three parts to postmodify the NPs with either PCBMA

brushes, mannose, or PEG. An increase in NP size from 497 nm to 539 nm was observed after functionalization with PCBMA. The zwitterionic PCBMA polymer chains can associate through inter- and intramolecular electrostatic interactions, which prevents the polymer from adapting a stretched conformation; upon further postmodification of PCBMA with amine-mannose, some of those zwitterionic associations are broken up, apparent from an increase in the thickness of the brush layer, resulting in a final NP size of 678 nm. The sizes of the NPs functionalized with PEG and mannose monolayers were 562 nm and 580 nm, respectively. Furthermore, we conducted ELS measurements to determine the zeta potential after postmodification of the PLGA particles (**Figure 3**). An increase in zeta potential was observed in all cases. Compared with unmodified PLGA nanoparticles, the zeta potential of the PCBMA-coated NPs increased from -33.6 mV to -19.2 mV. After conjugation of mannose to the PCBMA brushes, the zeta potential further increased to -14.2 mV because some of the carboxy-groups in the CBMA unit were used to bind amine-mannose, thus reducing the number of negative charges and increasing the zeta potential. Only a slight zeta potential increase from -33.6 mV to -26.4 mV was observed for NPs modified with PEG monolayers. In case of NPs functionalized with mannose monolayers, the zeta potential increased to -17.2mV.

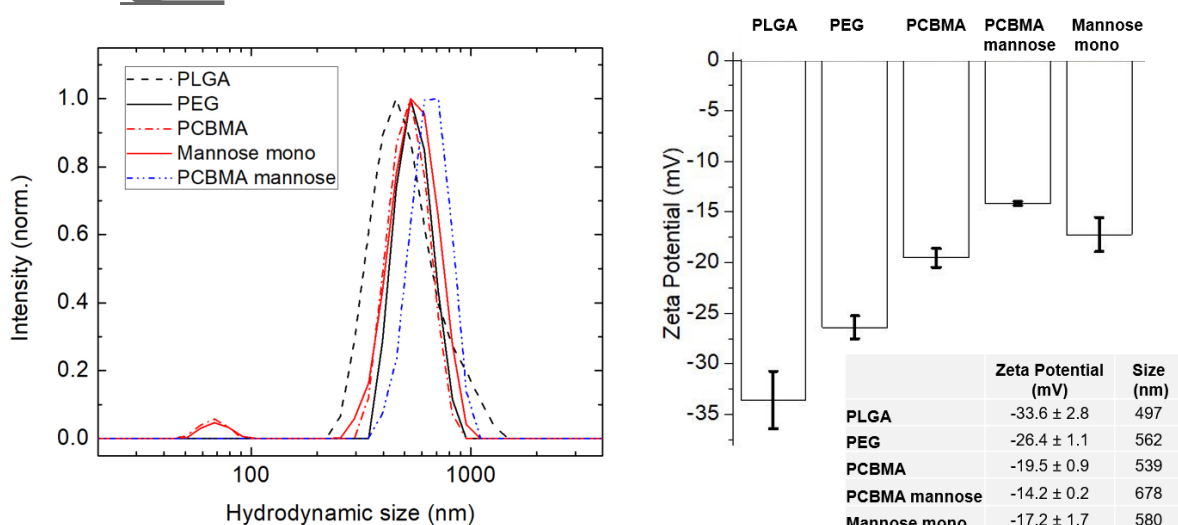|	Zeta Potential (mV)	Size (nm)
PLGA	-33.6 ± 2.8	497
PEG	-26.4 ± 1.1	562
PCBMA	-19.5 ± 0.9	539
PCBMA mannose	-14.2 ± 0.2	678
Mannose mono	-17.2 ± 1.7	580

Figure 3. Hydrated nanoparticle size of fluorescently labeled PLGA NPs and the same NPs after postmodification with PEG and mannose monolayers (Mannose mono), PCBMA brushes and PCBMA mannose brushes (PCBMA mannose) measured by DLS (left), and zeta potential values measured by ELS (right). The table summarizes the size and zeta potential values of the particle groups.

2.2. Cellular Uptake

When designing a macrophage-targeting nanoparticle drug delivery platform, it is essential to evaluate the macrophage-targeting ability of the NPs as well as their circulation life in the bloodstream. Since the main premise of the developed nanoparticle platform is the efficient targeting of macrophages, high NP uptake by the macrophages is critical and should be evaluated first and foremost. Therefore, we assessed the uptake of the different NP groups (NPs functionalized with PEG or mannose monolayers, or PCBMA mannose brushes) by RAW 264.7 macrophages. The PEGylated particles were included in this study as a baseline for nonspecific NP uptake. The main goal of this experiment was to determine whether the mannose brush coating would result in higher NP uptake levels than the mannose monolayer coating. The cells were incubated with the respective formulation in 96-well plates (10^8 particles per well) for 30 min and 5 h, and the NP uptake was analyzed by flow cytometry (**Figure 4**). The mechanisms of particle internalization have been established in literature,[54] and it was found that the primary uptake mechanism of nanoparticles (<1 μm size) by macrophages occurs via endocytosis; nanoparticles in the size range 300 – 500 nm (similar to the size range of the nanoparticles in our study) were more readily internalized by murine macrophages than particles with sizes below 150 nm.[55] Surprisingly, the mannose monolayer coatings did not improve the uptake of the NPs compared with PEG monolayer coatings; there was no significant difference between the uptake of PEG or mannose monolayer-coated nanoparticles by the macrophages, likely due to a low density of mannose groups. A significantly higher NP uptake (~4 times higher) by the macrophages was observed in case of the PCBMA mannose-coated nanoparticles; the uptake was high regardless of the incubation time (30 min, 5 h). We assume that this higher uptake is an effect of a higher density of mannose groups in case of the brush coating when compared to the monolayer coating. The improved uptake of the PCBMA mannose-coated nanoparticles compared with that of the PEGylated nanoparticles suggests that targeting of the macrophage mannose receptor plays a role.
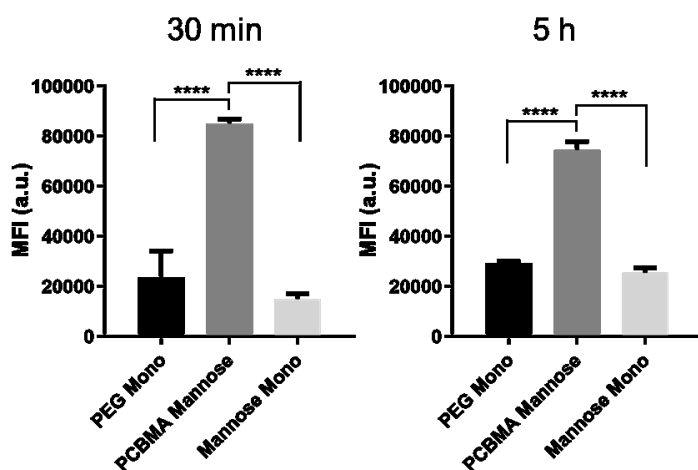
Figure 4. Uptake of fluorescently labeled PEG monolayer-, mannose monolayer-, and PCBMA mannose brush-modified nanoparticles (described in Figure 3) by RAW 264.7 macrophages after 30 min (left) or 5 h (right) incubation. The uptake values (MFI) were obtained by flow cytometry. Mean values were obtained from triplicates, and the data were analyzed by one-way ANOVA, followed by Tukey's post-test; P-values of <0.05 were considered statistically significant (*P < 0.05, **P < 0.01, ***P < 0.001; ****P < 0.0001), and P-values of >0.05 were considered not significant (ns).

2.3. Protein corona

As pointed out above, there are two critical parameters that determine the potential of a macrophage-targeting nanoparticle drug delivery platform: their macrophage-targeting ability (cellular uptake), and their circulation life in the bloodstream. After evaluating the NP uptake by the macrophages, the next step should be an assessment of their behavior in blood. This is important, because upon injection, blood proteins begin to adsorb to the NP surface and form a protein corona, which results in NP aggregation and rapid clearance by the liver. Therefore, we examined the behavior of the NPs in the presence of protein. In an initial experiment, we measured the zeta potential of the NPs in human serum albumin (HSA) to confirm the presence of a protein corona. In a second experiment, we evaluated the size of the different NPs in blood plasma (PLGA core + protein corona) over a time period of 15 h. Sine PEGylation is commonly employed to reduce, or even prevent, the formation of a protein corona, the PLGA NPs modified with PEG monolayers were used as the "gold standard" in this experiment.

As mentioned above, we first measured the zeta potential of the nanoparticles in HSA. The main motivation for this experiment was to confirm the presence of a protein corona; in addition, this experiment may provide a better understanding if (and to which extent) the absorption of protein would be affected by the different surface coatings. Blood serum contains mainly serum albumin, globulins, and fibrinogen, and we chose albumin as the most abundant protein in the human body at a concentration of 40 g L^{-1}. The zeta potential values were measured after a 30-min incubation period of the respective nanoparticle formulation in 40 g L^{-1} HSA (**Table 1**).

Table 1. Zeta potential values of the functionalized nanoparticles after a 30-min incubation in HSA (40 g L^{-1}), and zeta potential difference (Δ) obtained from a comparison of the zeta potential values in HSA with the zeta potential values measured prior to incubation with HSA.

	Zeta potential (mV) in HSA	Zeta potential difference (Δ, mV)
PLGA (no coating)	-3.4	30.2
PEG	-5.4	21.0
Mannose monolayer	-3.7	13.5
PCBMA mannose	-4.8	9.3

In all cases, an increase in the zeta potential was observed due to formation of a protein corona around the nanoparticles. The strongest increase from -33.6 mV to -3.4 mV (Δ=30.2 mV) was observed for unmodified PLGA nanoparticles, followed by NPs functionalized with PEG monolayers with a zeta potential increase of 21 mV. A lower value (Δ=9.3 mV) was observed in case of PCBMA mannose brushes. However, when comparing the actual zeta potential (instead of the Δ) of the different groups, they are very similar with values between -3.4 mV and -4.8 mV. The zeta potential values in HSA indicate that a protein corona is formed regardless of the surface coating, which was expected. However, the Δ values suggest that the surface coating may have an effect on the extent of protein adsorption to the NP surface. NPs modified with PCBMA mannose brushes had the lowest Δ value, which may indicate fewer albumin molecules attached to the surface compared with the other NP

groups. However, in case of the PCBMA-mannose brush coating, there is a possible scenario in which HSA molecules penetrate the brush layer rather than being adsorbed solely at the interface. Brushes can serve as 3D matrices allowing for smaller molecules to penetrate and get trapped. Unfortunately, it was not possible to accurately quantify the NP sizes in HSA by DLS due to formation of non-uniform aggregates. In addition, HSA and HSA aggregates scatter light; therefore, DLS might not be able to distinguish between the NPs and HSA aggregates. Among the different NPs, the PCBMA-mannose brush-coated nanoparticles showed the smallest change in zeta potential after incubation in HSA, which may imply that this coating was the most inert to protein adsorption. However, in reality, proteins other than albumin absorb onto the nanoparticle surface as well. And while the zeta potential measurements can provide some relevant information, they cannot be used to make a statement about the behavior of the NPs in blood. Additional methods are needed to more accurately reflect the NP behavior and protein corona formation in blood and to examine how the different NP coatings affect the protein-induced nanoparticle aggregation, as it will have implications for cellular uptake and targeting. As mentioned above, DLS cannot easily be used to evaluate the aggregation of NPs in protein-containing media, which also scatter light. This is not an issue for NTA (when used in fluorescent mode), as it allows for a visual analysis of NP aggregation in blood plasma.[49] We therefore employed NTA to further analyze the protein corona. The hard protein corona consists of blood components that exhibit strong interactions with the NP surface; soft protein coronas are formed by blood components with weak interactions with the NPs. Nonspecific binding of protein molecules to form a soft protein corona cannot be avoided even with PEGylated nanoparticles, which are designed to avoid protein adsorption.[56] It has been suggested that the morphology of the protein corona resembles an undefined, loose network of proteins, rather than a dense layer around the NPs.[57] NTA, as it is based on visual analysis, is therefore a perfect tool for further analysis of this loosely bound protein corona.

For further protein corona analysis, particles were incubated in blood plasma to simulate what they would be exposed to upon injection in the body. Particle size was evaluated using NTA at 0, 8, and 15 h time points. At 0 h, the size of the PEG monolayer-modified nanoparticles in plasma was significantly larger than that of the mannose monolayer- and PCBMA mannose-functionalized nanoparticles. Among all the groups, the size of the PCBMA mannose-modified nanoparticles in plasma was the smallest, suggesting the smallest protein corona; this result agrees with the zeta potential values in HSA, where PCBMA mannose-modified nanoparticles showed the smallest Δ

(suggesting less protein on the nanoparticle surface). This result could also explain why the cellular uptake was significantly higher for the PCBMA mannose-coated nanoparticles than the mannose monolayer-modified nanoparticles. Cellular uptake and targeting are strongly affected by the protein corona;[57] the larger protein corona of the mannose monolayer-modified particles may effectively act as a shield and thereby reduce, or even prevent, the mannose receptors from "seeing" the mannose moieties conjugated to the nanoparticle surface.

Previously published studies have suggested that the initial protein corona largely consists of albumin, whereas other proteins begin to adsorb, and potentially replace some of the albumin, at the nanoparticle surface at later time points.[58] At 8 h, the particle size increased for all groups, which may indicate that proteins other than albumin begin to adsorb. Over time, albumin is replaced by other proteins present in blood plasma;[58] this may explain the decrease in the protein corona sizes at 15 h when compared with the sizes at 8 h. The presence of the targeting moiety (mannose) did not lead to an increase in the particle size in blood plasma; there were no significant differences between the PEG monolayer-modified nanoparticles and the two mannosylated nanoparticle groups at 8 or 15 h. Similar to PEGylated nanoparticles, it should therefore be possible to employ the PCBMA mannose-functionalized nanoparticles as drug delivery vehicles.

2.4. Nanoparticle aggregation in blood plasma

Nanoparticle clearance by the liver is one of the major hurdles in nanomedicine and one of the reasons for the limited success of nanoparticle-based targeted drug delivery. The adsorption of blood proteins results in nanoparticle aggregation, and this apparent increase in NP size facilitates clearance from the bloodstream. Having evaluated the NP sizes in blood plasma (NP core + protein corona), we next aimed to quantify the NP aggregation in blood plasma. This is an essential experiment, as the aggregation of the NPs after injection into the bloodstream leads to their rapid clearance from the bloodstream. The ideal drug carrier should not aggregate upon injection and exhibit prolonged circulation in the bloodstream to reach its target. PEGylated NPs were used as the "gold standard", as PEGylation has been widely employed to prolong the NP circulation. The aggregation of the NPs in blood plasma was assessed using NTA in fluorescent mode. Videos were recorded after incubation of the NPs in blood plasma at different time points, and the analysis was carried out as described in the experimental section. The question we wanted to address by evaluating NP aggregation behaviors in

blood plasma was whether these particles can be used as drug carriers to target macrophages. Achieving a similar aggregation behavior as PEGylated nanoparticles is crucial to avoid clearance from the immune system upon particle injection. The number of particles in aggregates ranged from approximately 760 to 940 particles per 1×10^5 total particles with standard errors ranging from 140 to 250 particles. As shown in **Figure 5**, we found no significant difference in the number of particles in the aggregates of the evaluated functionalized nanoparticles in blood plasma. The PCBMA mannose-coated nanoparticles ($762 +/- 172$ particles per 1×10^5 total particles) showed the same aggregation behavior as the PEG monolayer-coated nanoparticles ($763 +/- 140$ particles per 1×10^5 total particles); larger aggregates were observed for the mannose monolayer-modified particles ($939 +/- 250$ particles per 1×10^5 total particles). As mentioned above, the outstanding circulation properties of PEGylated particles is well-known, and therefore, we would expect the PCBMA mannose-coated nanoparticles to behave similarly in the bloodstream after injection. Combined with the high uptake of these particles by macrophages, we believe that the PCBMA mannose-modified PLGA nanoparticles are promising candidates for targeted delivery of therapeutics to macrophages.
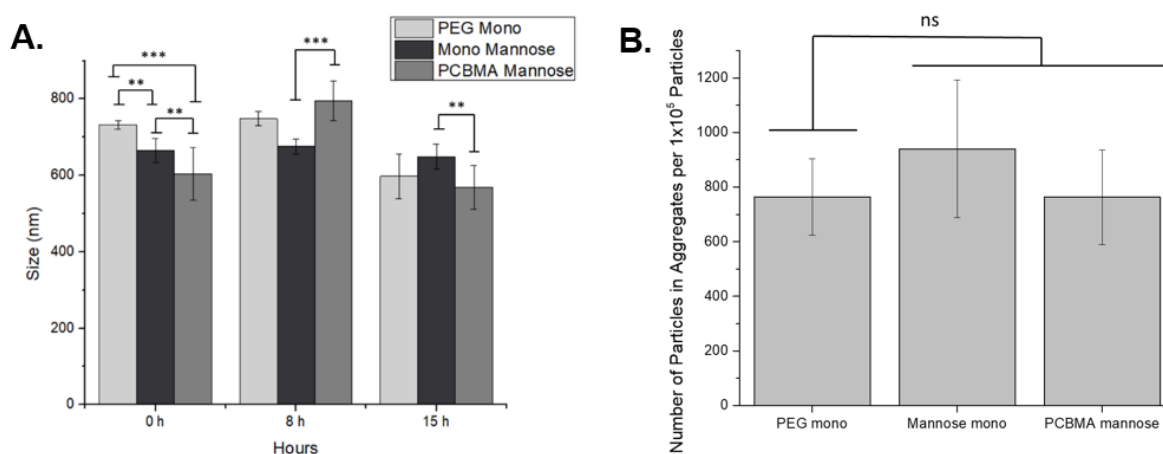

Figure 5. Evaluation of the PEG monolayer-, mannose monolayer-, and PCBMA mannose-modified nanoparticles in blood plasma: (A). Particle size (particle + protein corona) in blood plasma after 0, 8, and 15 h. (B.) Aggregation in blood plasma over a 24-h time period plotted as the number of particles in aggregates per 10^5 particles. The mean values in (A.) were obtained from the data from 9-14 videos for each time point. The mean values in (B.) were obtained from the data of four time points measured

over a 24-h period (0, 4, 15, 24 h). All data were analyzed by one-way ANOVA, followed by Tukey's multiple comparison test; P-values of < 0.05 were considered statistically significant (*P < 0.05, **P < 0.01, ***P < 0.001; ****P < 0.0001), and P-values of > 0.05 were considered not significant (ns). Error bars represent the standard error of the data sets. For (B.) the standard error was calculated from the pooled variance of the groups (the calculations can be found in the supporting information).

3. Conclusion

In summary, PLGA nanoparticles were fabricated by electrohydrodynamic jetting and postmodified with either PEG monolayers, mannose monolayers, or PCBMA mannose brushes. The aim of this work was to evaluate the potential of PCBMA mannose brush-functionalized particles to deliver therapeutics of interest to macrophages. We furthermore investigated the effect of the coating on the protein corona size and the nanoparticle aggregation in blood plasma, and the results were compared to PEGylated NPs as the "gold standard". Functionalization with PCBMA mannose brushes resulted in higher nanoparticle uptake by the macrophages than functionalization with mannose monolayers. In addition, the size of the PCBMA mannose-modified nanoparticles in blood plasma was smaller than that of the PEG- and mannose monolayer-coated nanoparticles, suggesting a smaller protein corona; however, there was no significant difference in the particle size in plasma at longer time scales. In terms of multicomponent aggregation in blood plasma, there was no significant difference between the PCBMA mannose-modified particles and PEGylated nanoparticles. All these results combined indicate that the PCBMA mannose brush-coated nanoparticles could potentially be used as drug delivery vehicles for targeting macrophages. Future studies will be needed to evaluate the *in vivo* performance of these particles, especially their *in vivo* targeting efficiency and blood circulation time.

4. Experimental Section
4.1. Materials and Methods

4.1.1. Materials

Poly(D,L-lactide-co-glycolic acid) PURASORB ® PDLG 5002A (PLGA) was a kind gift from Corbion and used as received. Poly(L-lactide)-bromoisobutyryl terminated (PLA(BiBB)) with an average molecular weight of 10,000-17,000 was obtained from Sigma Aldrich and used without any further purification. Cetyltrimethylammonium bromide (CTAB), (2-dimethylamino ethyl) methacrylate (DMAEMA), β−propiolactone, copper(I)bromide (CuBr), copper(II)bromide (CuBr$_2$), 2,2'-bipyridyl (Bipy), N-(3-Dimethylaminopropyl)-N′-ethylcarbodiimide hydrochloride (EDC), ethylenediaminetetraacetic acid (EDTA), Tween®20, methanol (MeOH), ethanol (EtOH), chloroform, dimethylsulfoxide (DMSO) and dimethylformamide (DMF) were obtained from Sigma Aldrich and used without further purification. N-hydroxysulfosuccinimide (sulfo-NHS) was purchased from Thermo Fisher Scientific and used without further purification. PBS buffer was obtained from Gibco. ADS133YE (poly[(9,9-dioctylfluorenyl-2,7-diyl)-alt-co-(1,4-benzo-(2,1',3)-thiadiazole)]) was ordered from American Dye Source, Inc. Amine-PEG$_{1k}$ was obtained from Nanocs. D-mannosamine hydrochloride was purchased from Sigma Aldrich. Raw 264.7 (ATCC® TIB-71^{TM}) cells were purchased from ATCC. Whole goat blood with Alsever's solution (an anticoagulant) was obtained from Lampire Biological Laboratories (catalog# 7202503) and was centrifuged when received to separate the blood plasma from blood cells.

4.1.2. Methods

Scanning electron microscopy (SEM): SEM images were recorded using a FEI Nova 200 Nanolab SEM/FIB at the Michigan Center for Materials Engineering at acceleration voltages of 5kV. Images were processed using FIJI (a distribution of ImageJ v1.53c) to obtain the respective nanoparticle size distribution.

Dynamic/electrophoretic light scattering (DLS/ELS): DLS/ELS measurements were carried out using a Zetasizer Nano ZS (Malvern Panalytical). DLS was employed to measure the particle size distribution in PBS buffer after particle collection. The reported average nanoparticle sizes were obtained from Gaussian fits of the DLS data using Origin8. ELS was employed to determine the zeta potential of the NPs. Three individual measurements were carried out per sample and averaged to determine the particle size and zeta potential.

Nanoparticle tracking analysis (NTA): NTA measurements were carried out with a Malvern Nanosight NS300 equipped with a syringe pump. NTA was employed to determine the

multicomponent aggregation of the nanoparticles in complex fluids and the particle size after incubation with blood plasma. The solutions were analyzed with a 488 nm laser using a 500 nm fluorescent filter (NTA was operated in fluorescence mode). In fluorescence mode, NTA analyzes only the fluorescent nanoparticles and avoids mischaracterization due to the proteins present in blood plasma, as it would occur in scatter mode. Samples were measured under flow such that particles were visible on the screen for 5-10 secs. On this specific instrument used in this study, that corresponded to a setting of 100 au on the syringe pump.

4.2. Nanoparticle fabrication and characterization

4.2.1. Nanoparticle fabrication

PLGA/PLA(BiBB) nanoparticles were fabricated by electrohydrodynamic jetting (illustrated in Figure 1). In the electrohydrodynamic jetting process, the polymer solution is pumped through a metal capillary connected to a conductive substrate. Applying high voltage (~12-15 kV) results in solvent evaporation and the formation of nanoparticles, which are sprayed onto the conductive substrate. The distance between the capillary tip and the collector sheet was adjusted to 30 cm. The polymer solution was prepared by dissolving the desired amounts of PLGA, PLA(BiBB) and CTAB in 70:30 v/v% chloroform/DMF. To fluorescently label the particles, the polymeric green dye ADS133YE was dissolved in chloroform (1 mg mL^{-1}) prior to preparing the polymer solution for electrojetting. We fabricated three different batches of PLGA nanoparticles with PLGA/PLA(BiBB) ratios of 5:5, 7.5:2.5 and 9:1 (w/w); each formulation contained 2.5 w/w% CTAB. The electrojetted nanoparticles were stored in vacuum for at least 2 weeks to remove any solvent residues. Then, the nanoparticles were collected with a razor blade and dispersed in PBS buffer containing 0.1% Tween20. Centrifugation was employed to separate larger (micron-sized) particles from the smaller nanoparticles. The nanoparticles were washed 10x with PBS and stored at 4°C until use.

4.2.2. Nanoparticle postmodification with PEG and mannose monolayers

PEG and mannose monolayer coatings were obtained by sulfo-NHS/EDC chemistry (Figure 1). Briefly, the nanoparticles were tip-sonicated in 1 mL of PBS containing 0.01 v/v% Tween20 to break

up aggregates which may have formed during storage. The particles were then incubated with 20 mg EDC for 20 min on a rotator to ensure continuous mixing, followed by a 20-min incubation with 20 mg sulfo-NHS. The nanoparticles were then recovered by centrifugation (12,700 RCF, 1 min) to remove any unreacted components and redispersed in PBS containing 0.01 v/v% Tween20. Next, the nanoparticles were tip-sonicated, and 10 mg of amine-functionalized component (amine-PEG$_{1k}$ or amine mannose) was added. The reaction was carried out for 2-3 h at room temperature on a rotator. The nanoparticles were cleaned by centrifuging and redispersing the pellet in PBS buffer 10x.

4.2.3. Nanoparticle postmodification with PCBMA mannose brushes

PCBMA brush coatings were synthesized by SI-ATRP. Prior to SI-ATRP, CBMA was synthesized according to literature procedure from DMAEMA and β-propiolactone (see supporting information).[38] SI-ATRP was carried out as follows: The nanoparticles were dissolved in 1.5 mL PBS containing 0.01 v/v% Tween20 in a Schlenk flask. The catalyst solution was prepared in a second Schlenk flask containing 0.068 g Bipy, 0.004 g CuBr$_2$ and 0.028 g CuBr dissolved in 3.2 mL MeOH. Both Schlenk flasks were deoxygenated by three freeze-pump-thaw cycles. The nanoparticles were then transferred to the Schlenk flask containing the catalyst solution under Argon using a syringe, and SI-ATRP was carried out for 120 mins. Afterwards, the polymerization solution was exposed to air to terminate the reaction. The nanoparticles were recovered by centrifuging the mixture for 1 min at 12,700 RCF. The resulting pellet was washed with 1M EDTA three times to remove any copper residues, then redispersed in PBS and washed with PBS 10x before use. NPs coated with PCBMA brushes were further postmodified to obtain the desired PCBMA mannose brush coatings. First, the pellet was tip-sonicated in 1 mL PBS containing 0.1 v/v% Tween20. The particles were incubated with 20 mg EDC for 20 min on a rotator. This incubation was followed by another incubation step with 20 mg sulfo-NHS for 20 min. The nanoparticles were recovered by centrifugation at 12,700 RCF for 1 min to remove unreacted components, redispersed in PBS containing 0.01 v/v% Tween20 and tip-sonicated. Then, 10 mg of amine-mannose was added, and the reaction was carried out for 2-3 h at room temperature on a rotator. The nanoparticles were recovered by centrifugation, redispersed in PBS and washed with PBS 10x.

4.2.4. Cellular uptake

Flow cytometry was carried out to evaluate the NP uptake by RAW 264.7 macrophages. The cells were seeded in a 96-well plate at a density of 100,000 cells per well in media supplemented with 10% FBS and 1% strep. After a few hours, NP formulations (10^8 particles per well) were added. After the desired incubation time (30 min or 5 h), the cells were washed with PBS three times, trypsinized, washed with PBS again twice and stained with DAPI. Next, the macrophages were analyzed with flow cytometry. A Cytoflex (Beckman Coulter) cell analyzer located at the flow cytometry core at the University of Michigan was used for all measurements, and data were analyzed using FlowJo software.

4.2.5. Nanoparticle aggregation in blood plasma

NTA was used to evaluate NP size and multicomponent aggregation after incubation with goat plasma. The NPs were incubated with plasma at 37°C over a period of 24 h on a water bath, and the concentration of the NPs was adjusted to achieve 8×10^8 particles mL^{-1} (ideal concentration range for NTA). After the different incubation periods proposed, the samples were analyzed with NTA. For each sample, 14 videos of 60 seconds were recorded. Any video that contained a 'high vibration' error (typically caused by the presence of a bubble disrupting the flow) was not used for size results. Only data points where at least 4 usable videos were collected were used, which is the recommended procedure for size analysis using the NTA.

For protein corona characterization, the size of particles was measured at the different time points after incubation with plasma by NTA 3.2 software provided by Malvern and the mean size of the particle was reported. The size of different particles was compared after incubation for 0, 8, and 15 hours with plasma. For multicomponent aggregation studies, NTA videos were visualized, and the number of particles in multicomponent aggregates was counted manually at each time point. An aggregate was identified as more than one particle center moving together without Brownian motion on the NTA videos. The number of particles per aggregate was compared with the total number of particles in the video. To compare the number of particles in the multicomponent aggregates, the samples were normalized to 10^5 particles.

4.2.6. Statistical analysis

All data were analyzed by one-way ANOVA, followed by Tukey's post-test; P-values of <0.05 were considered statistically significant (*P < 0.05, **P < 0.01, ***P < 0.001; ****P < 0.0001), and P-values of >0.05 were considered not significant (ns).

Supporting Information

Supporting Information is available from the Wiley Online Library or from the author.

Acknowledgements

References:

1.   J. K. Patra, G. Das, L. F. Fraceto, E. V. R. Campos, M. d. P. Rodriguez-Torres, L. S. Acosta-Torres, L. A. Diaz-Torres, R. Grillo, M. K. Swamy, S. Sharma, S. Habtemariam, H.-S. Shin, *J. Nanobiotechnology,* **2018**, *16*, 71.

2.   N. Habibi, D. F. Quevedo, J. V. Gregory, J. Lahann, *Wiley Interdiscip. Rev. Nanomed. Nanobiotechnol.,* **2020**, *12*, e1625.

3.   Y. Duan, A. Dhar, C. Patel, M. Khimani, S. Neogi, P. Sharma, N. Siva Kumar, R. L. Vekariya, *RSC Advances,* **2020**, *10*, 26777-26791.

4.   D. C. Luther, R. Huang, T. Jeon, X. Zhang, Y.-W. Lee, H. Nagaraj, V. M. Rotello, *Adv. Drug Deliv. Rev.,* **2020**, *156*, 188-213.

5.   N. Habibi, S. Christau, L. J. Ochyl, Z. Fan, A. Hassani Najafabadi, M. Kuehnhammer, M. Zhang, M. Helgeson, R. von Klitzing, J. J. Moon, J. Lahann, *Adv. Ther.* **2020**, *3*, 2000100.

6.   S. Sur, A. Rathore, V. Dave, K. R. Reddy, R. S. Chouhan, V. Sadhu, *Nano-Struct. Nano-Objects,* **2019**, *20*, 100397.

7.   D. N. Kapoor, A. Bhatia, R. Kaur, R. Sharma, G. Kaur, S. Dhawan, *Ther. Delivery,* **2015**, *6*, 41-58.

8.   I. Bala, S. Hariharan, M. N. Kumar, *Crit. Rev. Ther. Drug Carrier Syst.,* **2004,** *21*, 387-422.

9.   S. Acharya, S. K. Sahoo, *Adv. Drug Delivery Rev.,* **2011,** *63*, 170-183.

10.   J. Park, P. M. Fong, J. Lu, K. S. Russell, C. J. Booth, W. M. Saltzman, T. M. Fahmy, *Nanomedicine,* **2009,** *5*, 410-418.

11.   F. Sadat Tabatabaei Mirakabad, K. Nejati-Koshki, A. Akbarzadeh, M. R. Yamchi, M. Milani, N. Zarghami, V. Zeighamian, A. Rahimzadeh, S. Alimohammadi, Y. Hanifehpour, S. W. Joo, *Asian Pac. J. Cancer Prev.,* **2014,** *15*, 517-535.

12.   F. Alexis, E. Pridgen, L. K. Molnar, O. C. Farokhzad, *Mol. Pharmaceutics,* **2008,** *5*, 505-515.

13.   R. Gref, M. Lück, P. Quellec, M. Marchand, E. Dellacherie, S. Harnisch, T. Blunk, R. H. Müller, *Colloids Surf., B,* **2000,** *18*, 301-313.

14.   S. Parveen, S. K. Sahoo, *Eur. J. Pharmacol.,* **2011,** *670*, 372-383.

15.   D. M. Mosser, J. P. Edwards, *Nat. Rev. Immunol.* **2008,** *8*, 958-969.

16.   S. Chen, J. Yang, Y. Wei, X. Wei, *Cell. Mol. Immunol.* **2020,** *17*, 36-49.

17.   P. Chen, X. Zhang, A. Venosa, I. H. Lee, D. Myers, J. A. Holloway, R. K. Prud'homme, D. Gao, Z. Szekely, J. D. Laskin, D. L. Laskin, P. J. Sinko, *Pharmaceutics,* **2020,** *12*, 243.

18.   T. Mosaiab, D. C. Farr, M. J. Kiefel, T. A. Houston, *Adv. Drug Deliv. Rev.,* **2019,** *151-152*, 94-129.

19.   Y. Pei, Y. Yeo, *J. Controlled Release,* **2016,** *240*, 202-211.

20.   J. Li, Y. Wang, J. Yang, W. Liu, *Chem. Eng. J.,* **2021**, *420*, 127638.

21.   G. Pellizzari, H. J. Bax, D. H. Josephs, J. Gotovina, E. Jensen-Jarolim, J. F. Spicer, S. N. Karagiannis, *Trends Mol. Med.,* **2020**, *26*, 615-626.

22.   M. A. F. Yahaya, M. A. M. Lila, S. Ismail, M. Zainol, N. A. R. Nik Mohd Afizan, *J. Immunol. Res.,* **2019,** *2019*, 2368249.

23.   X. Zhang, W. Tian, X. Cai, X. Wang, W. Dang, H. Tang, H. Cao, L. Wang, T. Chen, *PloS One,* **2013,** *8*, e65896.

24.   J. M. Irache, H. H. Salman, C. Gamazo, S. Espuelas, *Expert Opin. Drug Delivery,* **2008,** *5*, 703-724.

25.   Q. Zhang, L. Su, J. Collins, G. Chen, R. Wallis, D. A. Mitchell, D. M. Haddleton, C. R. Becer, *J. Am. Chem. Soc.,* **2014,** *136*, 4325-4332.

26.   M. H. Xiong, Y. J. Li, Y. Bao, X. Z. Yang, B. Hu, J. Wang, *Adv. Mater.,* **2012,** *24*, 6175-6180.

27.   C. Fornaguera, G. Calderó, M. Mitjans, M. P. Vinardell, C. Solans, C. Vauthier, *Nanoscale,* **2015,** *7*, 6045-6058.

28.   L. Soddu, D. N. Trinh, E. Dunne, D. Kenny, G. Bernardini, I. Kokalari, A. Marucco, M. P. Monopoli, I. Fenoglio, *Beilstein J. Nanotechnol.,* **2020,** *11*, 550-567.

29.   R. Cukalevski, S. A. Ferreira, C. J. Dunning, T. Berggård, T. Cedervall, *Nano Res.,* **2015,** *8*, 2733-2743.

30.   G. Storm, S. O. Belliot, T. Daemen, D. D. Lasic, *Adv. Drug Deliv. Rev.,* **1995,** *17*, 31-48.

31.   Z. Hussain, S. Khan, M. Imran, M. Sohail, S. W. A. Shah, M. de Matas, *Drug Delivery Transl. Res.,* **2019,** *9*, 721-734.

32.   A. S. Zahr, C. A. Davis, M. V. Pishko, *Langmuir,* **2006,** *22*, 8178-8185.

33.   G. Cheng, G. Li, H. Xue, S. Chen, J. D. Bryers, S. Jiang, *Biomaterials,* **2009,** *30*, 5234-5240.
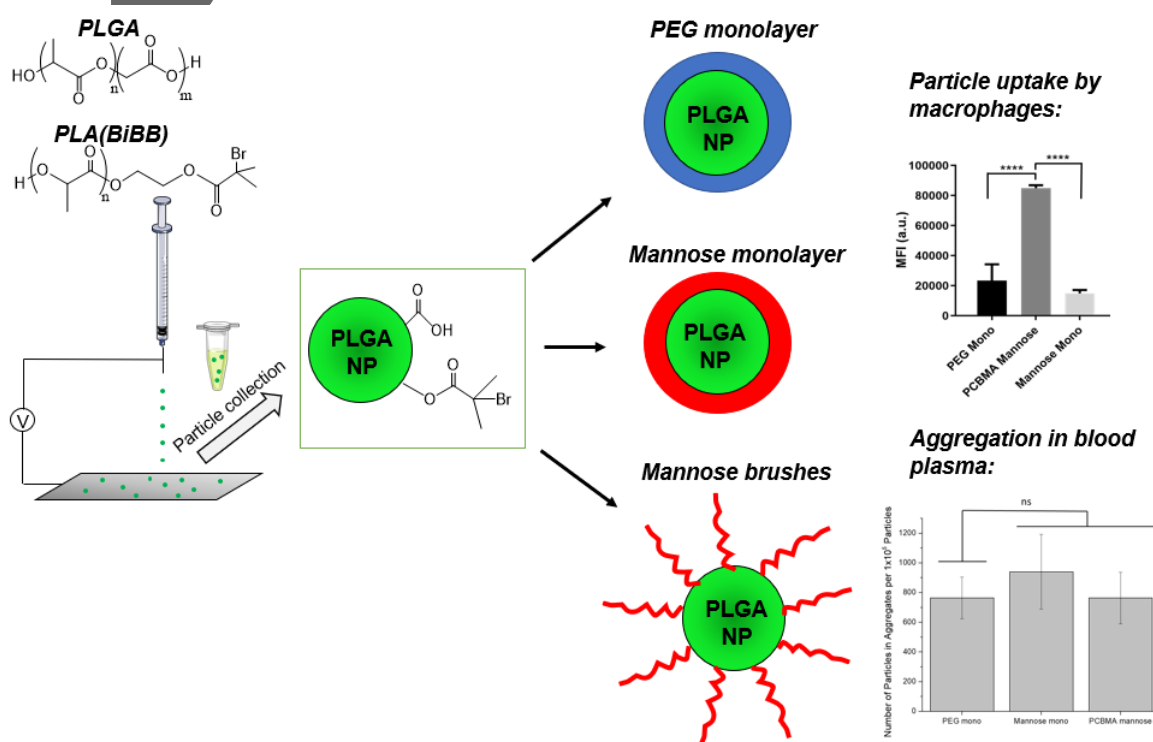
34.   X. Han, S. Li, X. Li, Q. Zhan, Y. Zhan, J. Zhao, X. Hou, X. Yuan, *J. Biomater. Appl.,* **2020,** *35*, 371-384.

35.   J. Jiang, J. Li, B. Zhou, C. Niu, W. Wang, W. Wu, J. Liang, *Polymers,* **2019,** *11*, 1019.

36.   C. Leng, H.-C. Hung, S. Sun, D. Wang, Y. Li, S. Jiang, Z. Chen, *ACS Appl. Mater. Interfaces,* **2015,** *7*, 16881-16888.

37.   C.-M. Xing, F.-N. Meng, M. Quan, K. Ding, Y. Dang, Y.-K. Gong, *Acta Biomater.,* **2017,** *59*, 129-138.

38.   Z. Zhang, S. Chen, S. Jiang, *Biomacromolecules,* **2006,** *7*, 3311-3315.

39.   J. Lahann, *Small,* **2011,** *7*, 1149-1156.

40.   S. Rahmani, S. Ashraf, R. Hartmann, A. F. Dishman, M. V. Zyuzin, C. K. Yu, W. J. Parak, J. Lahann, *Bioeng. Transl. Med.,* **2016,** *1*, 82-93.

41.   S. Bhaskar, K. M. Pollock, M. Yoshida, J. Lahann, *Small,* **2010,** *6*, 404-411.

42.   K.-H. Roh, D. C. Martin, J. Lahann, *Nat. Mat.,* **2005,** *4*, 759-763.

43.   S. Peng, B. Ouyang, Y. Men, Y. Du, Y. Cao, R. Xie, Z. Pang, S. Shen, W. Yang, *Biomaterials,* **2020,** *231*, 119680.

44.   X. Yao, S. Ma, S. Peng, G. Zhou, R. Xie, Q. Jiang, S. Guo, Q. He, W. Yang, *Adv. Healthcare Mater.,* **2020,** *9*, e1901582.

45.   R. Xie, P. Yang, S. Peng, Y. Cao, X. Yao, S. Guo, W. Yang, *J. Mater. Chem. B,* **2020**, *8*, 6128-6138.

46.   C. Weber, S. Morsbach, K. Landfester, *Angew. Chem. Int. Ed.,* **2019,** *58*, 12787-12794.

47.   S. Winzen, S. Schoettler, G. Baier, C. Rosenauer, V. Mailaender, K. Landfester, K. Mohr, *Nanoscale,* **2015,** *7*, 2992-3001.

48.   D. Griffiths, P. Carnell-Morris, M. Wright, in *Nanoparticles in Biology and Medicine*, Vol. 2118 (Eds: E. Ferrari, M. Soloviev), Humana, New York, NY **2020**, pp 289-303.

49.   M. S. Bannon, A. López Ruiz, K. Corrotea Reyes, M. Marquez, Z. Wallizadeh, M. Savarmand, C. A. LaPres, J. Lahann, K. McEnnis, *Part. Part. Syst. Charact.,* **2021**, *38*, 2100016.

50.   V. Filipe, A. Hawe, W. Jiskoot, *Pharm. Res.,* **2010,** *27*, 796-810.

51.   T. Betancourt, J. D. Byrne, N. Sunaryo, S. W. Crowder, M. Kadapakkam, S. Patel, S. Casciato, L. Brannon-Peppas, *J. Biomed. Mater. Res., Part A,* **2009,** *91*, 263-276.

52.   Y.-P. Li, Y.-Y. Pei, X.-Y. Zhang, Z.-H. Gu, Z.-H. Zhou, W.-F. Yuan, J.-J. Zhou, J.-H. Zhu, X.-J. Gao, *J. Controlled Release,* **2001,** *71*, 203-211.

53.   D. F. Quevedo, N. Habibi, J. V. Gregory, Y. Hernandez, T. D. Brown, R. Miki, B. N. Plummer, S. Rahmani, J. E. Raymond, S. Mitragotri, J. Lahann, *Macromol. Rapid Commun.,* **2020,** *41*, 2000425.

54.   F. Ahsan, I. P. Rivas, M. A. Khan, A. I. Torres Suarez, *J. Control. Release,* **2002,** *79*, 29-40

55.   C. He, Y. Hu, L. Yin, C. Tang, C. Yin, *Biomaterials,* **2010,** *31*, 3657-3666.

56.   M. Lundqvist, T. Cedervall, *Small,* **2020,** *16*, e2000892.

57.   M. Kokkinopoulou, J. Simon, K. Landfester, V. Mailänder, I. Lieberwirth, *Nanoscale,* **2017,** *9*, 8858-8870.

58.   M. Rahman, S. Laurent, N. Tawil, Y. L'Hocine, M. Mahmoudi, *Protein-Nanoparticle Interactions,* Springer: Berlin, Germany, **2013**.

Table of Contents Entry: In this study, the potential of poly(lactic-co-glycolic acid) nanoparticles with a functional coating of poly(zwitterion)-mannose brushes to target macrophages is examined. Furthermore, the aggregation behavior of the nanoparticles in blood plasma is evaluated to determine their potential to be employed as drug delivery vehicles.

S. Christau, A. López Ruiz, N. Habibi, J. Witte, M. S. Bannon, K. McEnnis*, J. Lahann*

Macrophage-Targeting Poly(lactide-*co*-glycolic acid) Nanoparticles Decorated with Multifunctional Brush Polymers